# ANALYSIS OF INTERLAYER SLIP EFFECT IN REINFORCED ASPHALT MIXTURE BRIDGE DECK PAVEMENT WITH CONCRETE STRUCTURES

Yangjun MENG[1,2,*], Can LI[3]

*One important reason of common defects for the asphalt mixture bridge deck pavement is its viscoelasticity and interlayer slip. Therefore, the uniaxial compression creep experiments were conducted on AC-13 asphalt mixture at different temperatures, and the experimental data was fitted using the Burgers model. The analysis showed that a significant influence on the creep performance of the asphalt mixture is the temperature. Secondly, based on the principles of elasticity and four basic assumptions, the slip theory of composite beams between asphalt mixture and concrete structures is proposed, and calculation formulas for the sliding displacement under several simple loads are derived. Finally, based on an example of the pavement renovation and the experimental data, a self programming was used for calculation and ANSYS modeling was used for verification. The interlayer slip mechanical properties of asphalt mixtures have been analyzed under the action of self weight. The analysis results indicate that the viscoelasticity and interlayer slip of asphalt mixture have a significant impact on its mechanical properties, and it should be considered in the design of asphalt mixture bridge deck pavement.*

**Keywords:** Asphalt mixture; Creep; Interlayer Slip; Shear Force; Concrete Structures

## 1. Introduction

Currently, after a period of operation, the asphalt mixture pavement of concrete bridges exhibits problems like cracking, potholes, and rutting due to various reasons. These issues significantly affect the performance of the asphalt mixture pavement and, in severe cases, may endanger the structural safety of the bridge. Among them, The viscoelasticity of the asphalt mixture and interlayer slip are very important factors.

Tabasi et al.[1] studied the short-term and long-term cracking behavior of asphalt pavements under tensile and tearing deformation. Kuchiishi et al.[2] conducted research on the impact of the viscoelasticity of cold-recycled asphalt mixtures on pavement response. Zhu[3] established a viscoelastic constitutive model for asphalt concrete related to temperature and a coupled simulation system

[1] Changde College, Changde, Hunan, 415000, China. email: 352357749@qq.com
[2] Hunan University of Arts and Science, Changde, Hunan, 415000, China
[3] Furong College, Hunan University of Science and Arts, Changde, Hunan, 415000, China

of tire and road to analyze the distribution of wheel tracks under dynamic and static loads and the dynamic response of the pavement during vehicle braking. Benaboud et al.[4] proposed a new method for analyzing two-point bending (2 PB) fatigue test data on French standardized trapezoidal specimens according to European Standard EN 12697-24. Zhai et al.[5] selected a 70# base asphalt and analyzed the temperature sensitivity of Superpave asphalt using the HR-3 experimental system, focusing on the temperature sensitivity in the low and medium temperature ranges. Yang et al.[6] analyzed the function relationship between the loss factor and storage modulus of the FDZ model, which is independent of the time parameter. They established the main curve of viscoelastic parameters for the FDZ model, conducted validation, and compared it with the main curve of the Sigmoidal model. Pan et al.[7] carried out static load creep tests on asphalt pavements at different temperatures and axle loads based on the three-dimensional linear viscoelastic constitutive theory. They established a strain prediction method for the asphalt layer based on the three-dimensional viscoelastic constitutive relationship. You et al.[8] made indoor-formed double-layer asphalt mixture specimens and conducted experiments to explore the creep properties of the double-layer composite asphalt mixture. Mao [9] performed dynamic modulus, dynamic resilience modulus, and creep compliance tests on asphalt concrete of different structural layers to study and analyze the impact of viscoelastic parameters of asphalt mixtures under different loading methods on the mechanical response of pavement structures. Ma[10] chose high-resilience asphalt mixtures and tested their viscoelastic deformation behavior dynamically (dynamic modulus test) and statically (uniaxial penetration creep test) to study the viscoelastic properties of asphalt mixtures. Underwood and others[11-12] proposed a viscoelastic damage model for asphalt mixtures based on fracture mechanics and continuum mechanics and developed a computational program. Robert and others[13] explored the influence of porosity and filler type on the basic fracture limits of mastic and asphalt mixtures based on indoor tests. Hosseini et al.[14] studied the rheological properties of asphalt by adding carbon black and hydrocarbon additives. SALEH et al.[15] investigated the impact of long-term aging under real traffic and thermal conditions on the performance of asphalt mixture pavements. Kim et al. [16] researched the impact of uneven temperatures on the paving process of asphalt mixtures. Hesami et al.[17] proposed an empirical framework to determine the variation of asphalt mastic viscosity with mineral filler concentration. Ali et al. [18] conducted studies on foam warm mix asphalt and workability evaluation.

Liu[19] made asphalt concrete wheel-rolled specimens and Marshall specimens with different layer positions of geogrid reinforcement and analyzed the internal rules of the influence of geogrid layer position on the mechanical properties of reinforced asphalt concrete. Zha et al.[20] selected common reinforcement materials such as twisted steel wire mesh, self-adhesive fiberglass geogrid, steel-

plastic composite geogrid, and polycool long filament geotextile, and conducted performance tests of indoor reinforced composite specimens to analyze and compare the road performance and differential settlement resistance of different reinforced composite specimens.

In summary, it is not difficult to see that the viscoelasticity of asphalt mixtures is a key and challenging aspect of their mechanical performance analysis. Many scholars have conducted research in this area, mainly focusing on indoor experiments, pavement structure, and simulation analysis. Regarding reinforced asphalt mixture pavement for bridges, there is even less research considering viscoelasticity, especially on the mechanical properties of the interface between concrete structures and asphalt mixtures. Therefore, conducting theoretical analysis on the interlayer slip effect of reinforced asphalt mixture pavement and concrete structure layers aims to delve deeper into the binding performance and mechanism of concrete-asphalt mixtures.

## 2. Viscoelastic Effects of Asphalt Mixtures

To study the viscoelastic effects of AC-13 type asphalt mixtures, uniaxial compression creep tests were conducted at -10°C, -5°C, and 15°C. The experimental equipment consisted of a UTM-100 environmental chamber and loading apparatus. The specimen preparation method and parameters were as follows:

Cylindrical specimens (170mm in height and 150mm in diameter) were formed and cured, then cut to produce test specimens with a height of 100mm and a diameter of 100mm.

The results of the uniaxial compression creep tests of the AC-13 type asphalt mixtures at -10°C, -5°C, and 15°C are shown in Fig.1.

For ease of subsequent analysis and referencing relevant literature, the Burgers model was used to fit the above experimental data. The calculated results are shown in Table 1, and Fig.1 and Fig.2.

*Table 1*

**Fitting Parameters of Burgers Model**

| test temperature | $E_1$ /MPa | $\eta_1$ /MPa.s | $E_2$ /MPa | $\eta_2$ /MPa.s |
|---|---|---|---|---|
| -10℃ | 3904.790 | 6955359.637 | 2456.123 | 359125.591 |
| -5℃ | 2907.488 | 5178927.594 | 1828.817 | 267403.201 |
| 15℃ | 620.244 | 3314406.216 | 390.135 | 57044.167 |

Note: The constitutive equation of the Burgers model is $\sigma + \left(\frac{\eta_1}{E_1} + \frac{\eta_1+\eta_2}{E_2}\right)\dot{\sigma} + \frac{\eta_1 \cdot \eta_2}{E_1 E_2}\ddot{\sigma} = \eta_1\dot{\varepsilon} + \frac{\eta_1 \cdot \eta_2}{E_2}\ddot{\varepsilon}$, and the correlation coefficients of curve fitting are all greater than 0.995.

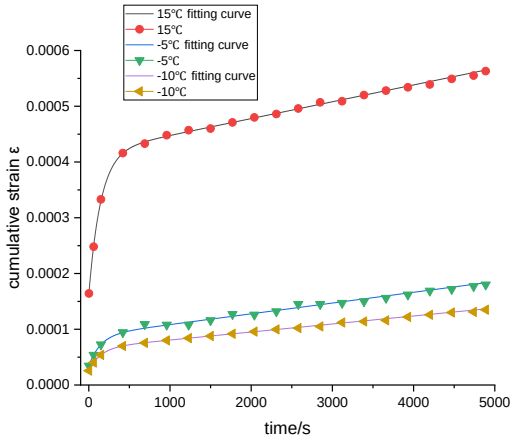


Fig. 1. Axial compression creep test curve and fitting curve of AC-13 asphalt mixture

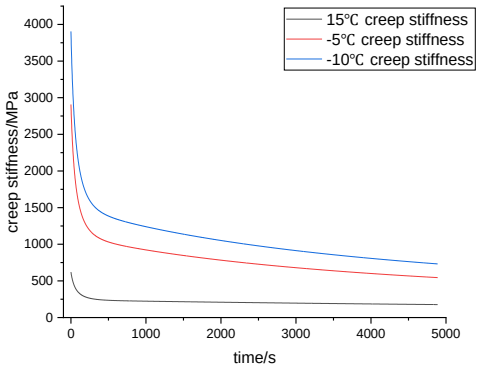


Fig. 2. Fitting curve of creep stiffness of AC-13 asphalt mixture under axial compression

According to Fig.1, it is evident that the axial creep of the asphalt mixture consists of three distinct stages. With the increase in loading time, the cumulative strain gradually increases until it reaches a stable value, undergoing an elastic phase, a viscoelastic phase, and a steady phase.

From Fig.2, it can be seen that as the temperature decreases, the creep stiffness gradually increases and the creep performance decreases. The creep stiffness at -5°C and 15°C is respectively 25.5% and 75.8% lower than that at -10°C, indicating that temperature significantly impacts the creep performance of asphalt mixtures. At different temperatures, the cumulative strains of the asphalt mixtures show clear differences, following the trend $\Sigma\varepsilon_{15℃}>\Sigma\varepsilon_{-5℃}>\Sigma\varepsilon_{-10℃}$. As time progresses, they eventually stabilize. Compared to the cumulative strain at 15°C, the cumulative strains at -5°C and -10°C are reduced by 68.0% and 76.0%, respectively.

## 3. Slip Theory of Asphalt Mixture-Concrete Composite Beams

### 3.1 Basic Assumptions

The static loading test results of asphalt mixture-concrete composite beams show that at the initial stage of loading, the interface of the composite beam deforms synergistically without any slip. As the deformation progresses, slip occurs at the interface until failure. Significant deformation occurs before failure, showing certain plastic development.

Based on the above analysis and existing research, the following assumptions are proposed:

①The concrete part of the composite beam behaves elastically and satisfies the plane section assumption.

②The shear-slip relationship at the interface satisfies $Q=ks$, where k is the shear slip stiffness, assumed to be consistent in both the compression and tension areas of the interface.

③Neglect various adverse effects caused by the slip behavior at the interface of the asphalt mixture-concrete composite beam for comprehensive analysis.

④Ignore the effects of shear deformation and the uplift forces at the interface.

### 3.2 Establishment of the Differential Equation

For ease of analysis, an infinitesimal element is selected from within the composite beam, divided into two isolated bodies for analysis: one being the asphalt mixture part (upper part), and the other the concrete part (lower part), which are then numbered (see Fig.3). The following balance equation is derived from the force analysis:

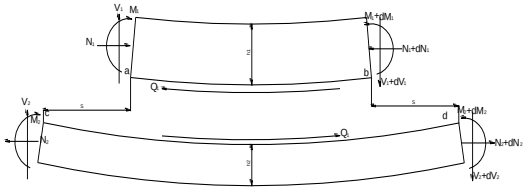

Fig. 3. Load analysis of asphalt mixture concrete composite beam

$$\begin{aligned} dM_1 - V_1 dx - \frac{1}{2} Q_1 h_1 dx = 0 \\ dM_2 - V_2 dx - \frac{1}{2} Q_1 h_2 dx = 0 \end{aligned} \tag{1}$$

In Equation (1): $M_1$, $V_1$, $M_2$, $V_2$ are the bending moments and shear forces acting on isolated bodies 1 and 2, respectively; $h_1$, $h_2$ are the heights of isolated bodies 1 and 2; $Q_1$ is the shear force at the tension zone interface.

From the differential equation (1), we get:

$$\frac{d\left(M_1+M_2\right)}{dx}-\left(V_1+V_2\right)-\frac{1}{2}Q_1\left(h_1+h_2\right)=0 \tag{2}$$

Let $M_1+M_2=M$, $V_1+V_2=V$, $Z_1=(h_1+h_2)/2$, then the equation can be transformed into:

$$\frac{dM}{dx}-V-Q_1Z_1=0 \tag{3}$$

According to elementary beam theory, curvature $\phi=\frac{M_1}{E_1I_1}=\frac{M_2}{E_2I_2}$ , $E_i$ is the modulus of elasticity, $I_j$ is the moment of inertia of the section. Combining with the Equation (3), the following equation can be derived:

$$EI\frac{d\phi}{dx}-V-Q_1Z_1=0 \tag{4}$$

In Equation (4): $EI$ is the bending stiffness of the composite section, calculated with isolated body 2 as the standard, $E_2I=E_2\left(\frac{I_1}{n}+I_2+\frac{d^2A_1A_2}{A_1+nA_2}\right)$ , where: $n=E_2/E_1$, $d$ is the distance between the centroids of isolated bodies 1 and 2, for a rectangular section, $d= Z_1$.

Slip is a common phenomenon, originating from different deformations on both sides, and the difference formed is the so-called slip displacement. Combining with Fig.3, we get $ds/dx=\varepsilon_{ab}-\varepsilon_{cd}$. Considering assumption 3 and analyzing the relationship between axial forces and deformation of the isolated bodies, we get:

$$\frac{ds}{dx}=\phi Z_1-\left(\frac{N_1}{E_1A_1}+\frac{N_2}{E_2A_2}\right) \tag{5}$$

In Equation (5): $s$ is the interface slip displacement; $N_1$, $N_2$ are the axial forces acting on isolated bodies 1 and 2. Combining with the section equilibrium condition, $N_1= N_2=A_2d_2M_z/I=A_1d_1M_z/nI$, where $A_1$, $A_2$ are the areas of isolated bodies 1 and 2; $d_1$, $d_2$ are the distances from the centroids of the sections of isolated bodies 1 and 2 to the centroid of the composite section; $M_z$ is the overall bending moment borne by the composite section.

Differentiating Equation (5) and considering the balance equation of the individual isolated body $\frac{dN_1}{dx}=\frac{dN_2}{dx}=-Q_1$ ,we get $\frac{d^2s}{dx^2}-\left(\frac{1}{E_1A_1}+\frac{1}{E_2A_2}+\frac{Z_1^2}{EI}\right)ks=\frac{V}{EI}Z_1$, let $\alpha^2=\left(\frac{1}{E_1A_1}+\frac{1}{E_2A_2}+\frac{Z_1^2}{EI}\right)k$ , $\beta=\frac{Z_1}{\left(\frac{EI}{E_1A_1}+\frac{EI}{E_2A_2}+Z_1^2\right)k}$ , we obtain:

$$\frac{d^2s}{dx^2}-\alpha^2s=\alpha^2\beta V \tag{6}$$

The general solution of Equation (6) is $s = c_1 e^{\alpha x} + c_2 e^{-\alpha x} - \beta V$ , where $c_1$, $c_2$ are arbitrary constants. Taking a simply supported beam as an example and combining the boundary conditions $s(x=0)=0$ and $s(x=L)=0$, the theoretical solution of slip displacement under different loading conditions can be determined. The calculation results under several special conditions are as follows:

1）Uniform load q:

$$s = \beta q\left[\frac{\mathrm{sh}\alpha(L/2-x)}{\alpha ch(\alpha L/2)} - \frac{L}{2} + x\right] \tag{7}$$

2）Concentrated load P：

$$s = \begin{cases} \dfrac{\beta P}{2}\dfrac{ch\alpha x}{ch(\alpha L/2)} - \beta V, V = \dfrac{P}{2}, x \in (0, L/2) \\ -\dfrac{\beta P}{2}\dfrac{ch\alpha x}{ch(\alpha L/2)} - \beta V, V = -\dfrac{P}{2}, x \in (L/2, L) \end{cases} \tag{8}$$

According to $\Delta\varepsilon = \dfrac{ds}{dx}$, the corresponding interface strain difference solution can be determined, with specific expressions omitted.

## 4. Analysis and Verification

Yingbin Avenue Elevated Bridge's right span YY6 is a 3×30m equal section single box double cell continuous beam bridge, located on a downhill section. Due to reasons like over-limit vehicles, construction, and operational maintenance, severe pavement distress was observed in this span. As a solution, the original pavement layer was modified using a 10 cm AC13 modified asphalt mixture with a layer of fiberglass geogrid at the bottom.

Combining experimental data, the viscoelastic effect under the self-weight of asphalt mixture was analyzed using a self-written program, with verification through ANSYS modeling (ANSYS model shown in Fig.4). The calculation model and corresponding overall analysis and calculation results are shown in Fig.5.

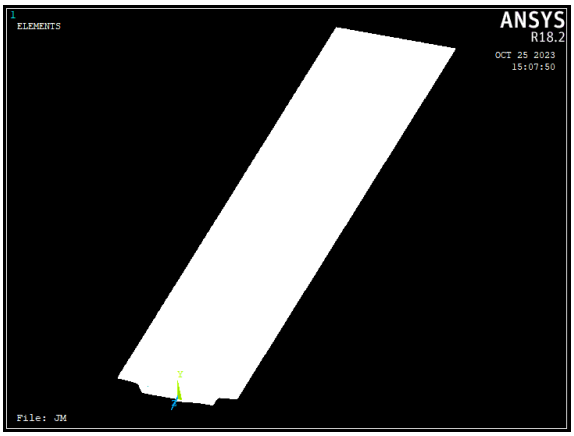


Fig. 4. ANSYS calculation model

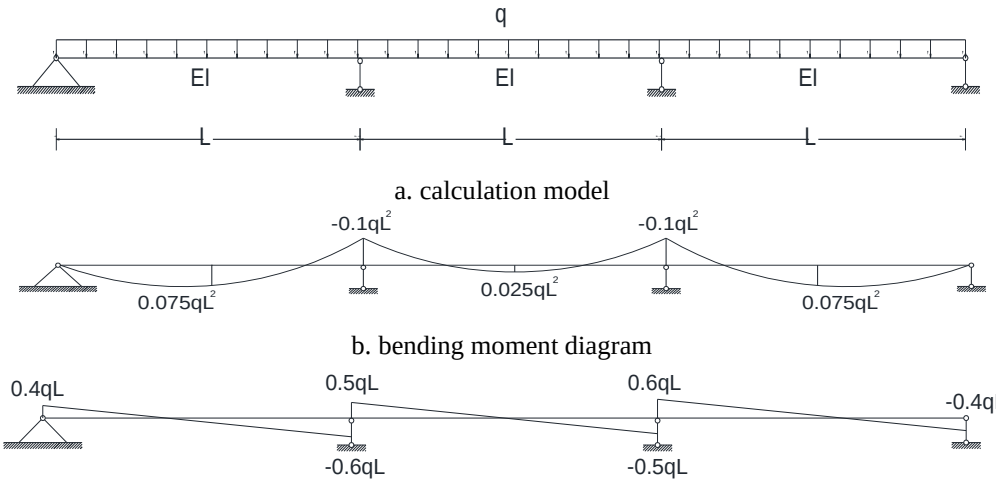


a. calculation model

b. bending moment diagram

c. shear force diagram

Fig. 5. Overall analysis and calculation results

Based on the theory presented in this article and combined with boundary conditions, the theoretical solutions for the slip displacement of asphalt mixture under the self weight (uniformly distributed load) of a 3×30m equal section continuous beam bridge are as follows:

First span: $s = c_1 e^{\alpha x} + c_2 e^{-\alpha x} - \beta q(0.4L - x)$, $x \in (0, L)$,

$$\text{Where: } c_1 = -\frac{11\alpha L ch(1.5\alpha L) + 5e^{-2.5\alpha L} + 5e^{-0.5\alpha L}}{20\alpha ch(\alpha L) ch(1.5\alpha L)}\beta q,$$

$$c_2 = -\frac{11\alpha L ch(1.5\alpha L) - 5e^{2.5\alpha L} - 5e^{0.5\alpha L}}{20\alpha ch(\alpha L) ch(1.5\alpha L)}\beta q.$$

Second span: $s = c_1 e^{\alpha x} + c_2 e^{-\alpha x} - \beta q(0.5L - x)$, $x \in (0, L)$, Where:

$$c_1 = -\frac{\beta q e^{-0.5\alpha L}}{2\alpha ch(1.5\alpha L)},\ c_2 = \frac{\beta q e^{0.5\alpha L}}{2\alpha ch(1.5\alpha L)}.$$

Third span: $s = c_1 e^{\alpha x} + c_2 e^{-\alpha x} - \beta q(0.6L - x),\ x \in (0, L)$, Where:

$$c_1 = \frac{11\alpha L\left(e^{-2.5\alpha L} + e^{0.5\alpha L}\right) - 10e^{-0.5\alpha L} - 10e^{1.5\alpha L}}{40\alpha ch(\alpha L)ch(1.5\alpha L)}\beta q,$$

$$c_2 = \frac{11\alpha L\left(e^{2.5\alpha L} + e^{-0.5\alpha L}\right) + 10e^{0.5\alpha L} + 10e^{-1.5\alpha L}}{40\alpha ch(\alpha L)ch(1.5\alpha L)}\beta q.$$

The above results have been validated by simulation analysis with ANSYS Software, indicating that the theoretical analysis is correct and reliable.

Basing the mechanical performance parameters of the 15°C asphalt mixture and ignoring shear slip, the calculation results of the interlayer shear force $Q_1$ between the concrete box girder and the asphalt mixture are shown in Fig.6.

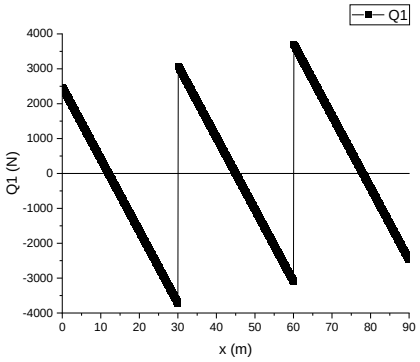


Fig. 6. Interlayer shear force $Q_1$ between concrete box girder and asphalt mixture (without slip)

From Fig.6, it can be seen that when there is no slip between the interface of the concrete box girder and the asphalt mixture, the interlayer shear force distribution is similar to the overall analysis shear force diagram, exhibiting a linear distribution along the length of beam, and $Q_1=VS/I$, which conforms to the basic rules of sectional shear force distribution in material mechanics.

Considering the interlayer slip, for ease of analysis, the mechanical performance parameters of the 15°C asphalt mixture were chosen. Based on the slip theory of the asphalt mixture-concrete composite beam, the slip displacement at the interface between the concrete box girder and the asphalt mixture is shown in Fig.7.

From Fig.7, it is apparent that when considering slip, the distribution patterns of the sliding displacement *s* and the interlayer shear force *ks* between the interface of the concrete box girder and the asphalt mixture are similar and significantly different from the case without slip consideration. A nonlinear distribution is observed along the length of the beam, with the maximum relative slip at each support point, gradually decreasing towards the inner span on both

sides. As the slip between the two interfaces consumes the work done by external forces, the interlayer shear force *ks* in the case of slip is significantly lower than the interlayer shear force $Q_1$ without slip consideration. The above conclusions have been confirmed once again by simulation analysis with ANSYS software.

The *s*-*x* curve and the *ks*-*x* curve are similar in shape and are symmetric about the Y-axis at *x*=45m.

Analysis shows that the slip displacement *s* and interlayer shear force *ks* exhibit a trend of small in the middle and large at both ends in the first and third span; but the slip displacement *s* and interlayer shear force *ks* exhibit a linear pattern in second span.

For the convenience of analysis and description, parameter sensitivity analysis was conducted at x=4.1m, 15m, and 24.7m positions.

Keeping the elastic modulus *E* of asphalt mixture constant, different shear slip stiffnesses *k* were selected for analysis at *x*=4.1m, 15m, and 24.7m. The calculation results of the sliding displacement *s* and interlayer shear force *ks* are shown in Fig.8 and Fig.9.

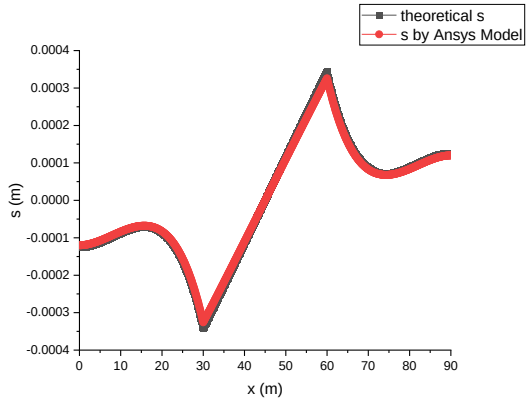


Fig. 7. Interlayer sliding displacement *s* between concrete box girder and asphalt mixture

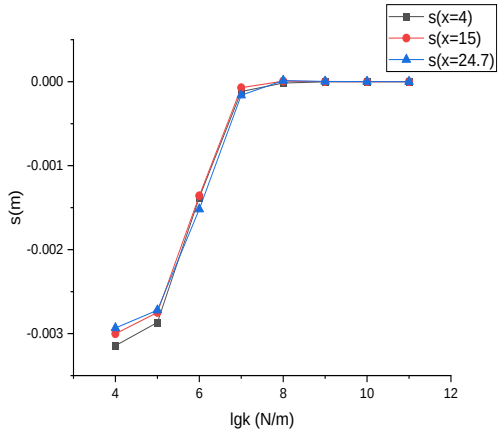


Fig. 8. Relationship curve between sliding displacement *s* and shear slip stiffness *k*

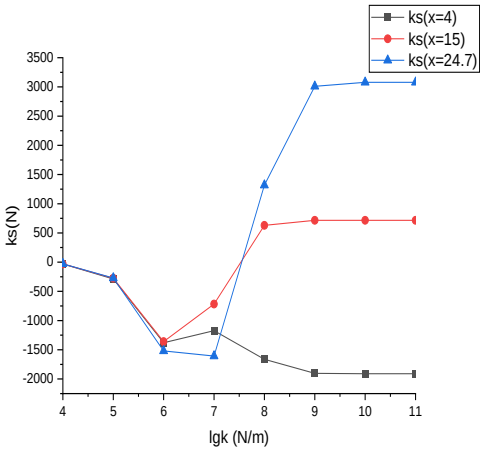


Fig. 9. Relationship curve between interlayer shear force *ks* and shear slip stiffness *k*

From Fig.8 and Fig.9, it can be deduced that there is a nonlinear relationship between the sliding displacement *s*, interlayer shear force *ks*, and the shear slip stiffness *k* at the interface between the concrete box girder and the asphalt mixture. As the shear slip stiffness *k* increases, the absolute value of sliding displacement *s* gradually decreases, eventually approaching zero.

In line with the above analysis, as the shear slip stiffness *k* increases, the absolute value of interlayer shear force *ks* gradually increases, eventually stabilizing at a value, namely the interlayer shear force $Q_1=VS/I$ without considering slip.

Also, as evident from the figures, the direction of slip varies at different locations, which is related to boundary conditions and the type of load.

Based on the uniaxial compression creep experiment results of the 15°C asphalt mixture, keeping the shear slip stiffness *k* constant and with the increase in time *t*, the sliding displacement *s* and interlayer shear force *ks* at *x*=4.1m, 15m, and 24.7m are shown in Fig.10 and Fig.11.

From Fig.10 and Fig.11, it can be seen that there is a nonlinear relationship between the sliding displacement *s*, interlayer shear force *ks*, and time *t* at the interface between the concrete box girder and the asphalt mixture. As time *t* increases, both the sliding displacement *s* and the interlayer shear force *ks* gradually decrease, eventually stabilizing. The *s*-*t* curve and the *ks*-*t* curve have similar shapes, each comprising three stages: a linear development stage, a creep strengthening stage, and a stable stage.

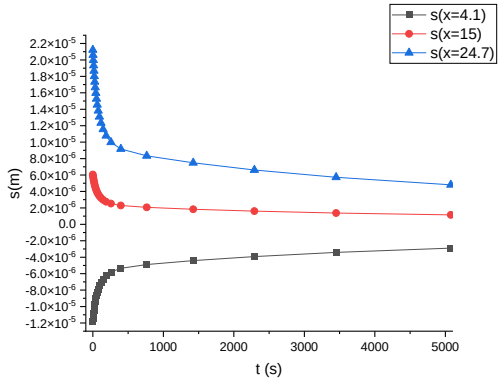


Fig. 10. Relationship curve between sliding displacement *s* and time

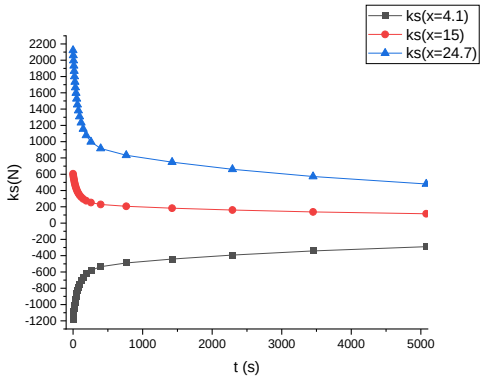


Fig. 11. Relationship curve between interlayer shear force *ks* and time

Keeping the shear slip stiffness *k* constant and with decreasing temperature, the sliding displacement *s* and interlayer shear force *ks* at *x*=4.1m, 15m, and 24.7m are shown in Fig.12 and Fig.13.

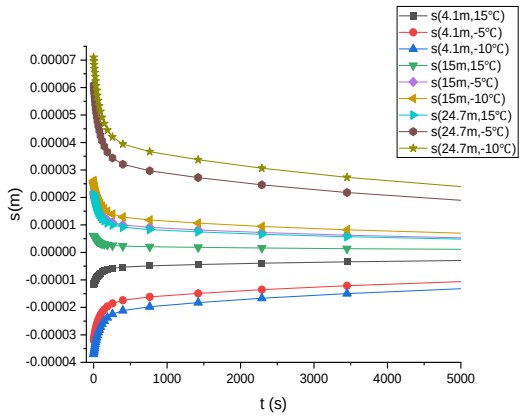


Fig. 12. Relationship curve between sliding displacement *s* and time at *x*=4.1m, 15m and 24.7m

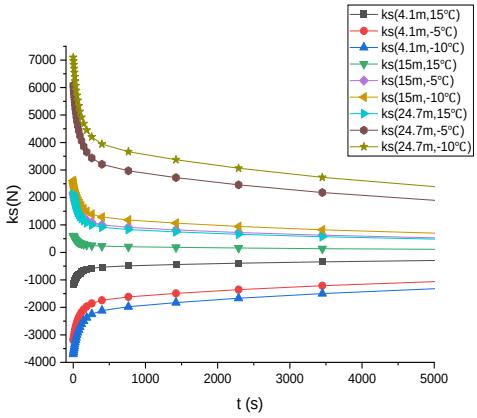


Fig. 13. Relationship curve between interlayer shear force *ks* and time at *x*=4.1m, 15m and 24.7m

From Fig.12 and Fig.13, it is clear that at *x*=4.1m, 15m, and 24.7m, the *s-t* curves and *ks-t* curves at the interface between the concrete box girder and the asphalt mixture resemble each other and are similar to the cumulative strain versus time curves of the asphalt mixture. At the same time, with increasing temperature, the absolute values of the sliding displacement *s* and the interlayer shear force *ks* gradually decrease. Based on the -10°C data, the maximum differences are 77.98% at *x*=4.1m, 83.54% at *x*=15m, and 79.78% at *x*=24.7m. As time progresses, the sliding displacement *s* and the interlayer shear force *ks* at each location gradually decrease, eventually stabilizing.

## 5. Conclusion

1. Uniaxial compression creep experiments of AC-13 asphalt mixture at different temperatures were carried out, and the experimental data were fitted using the Burgers model. As the temperature decreases, the creep stiffness gradually increases, and the creep performance gradually decreases. At different temperatures, the cumulative strains of asphalt mixtures show notable differences, following the trend $\Sigma\varepsilon_{15^{\circ}C}>\Sigma\varepsilon_{-5^{\circ}C}>\Sigma\varepsilon_{-10^{\circ}C}$.

2. Utilizing principles of elastic mechanics and based on four basic assumptions, the slip theory of asphalt mixture-concrete composite beams was proposed, deriving formulas for calculating sliding displacements under various simple loadings, and verified numerically using ANSYS models.

3. Combining the right span YY6 of Yingbin Avenue Elevated Bridge and uniaxial compression creep experiment data of AC-13 asphalt mixture, calculations were made using a self-written program, verified through ANSYS modeling. The mechanical performance of interlayer slip under the self-weight of the asphalt mixture, considering viscoelastic effects, was analyzed. The analysis results indicate that the viscoelasticity and interlayer slip of asphalt mixture have a significant impact on its mechanical properties, and it should be considered in the design of asphalt mixture bridge deck pavement.

## Acknowledgement

This research was supported by the Hunan Provincial Natural Science Foundation Project (2021JJ50136).

## R E F E R E N C E S

[1] Tabasi Ehsan, Zarei Mohammad, Naseri Alireza, Gashin Hosseini Seyedeh, Mirahmadi Majid, et al. Low temperature cracking behavior of modified asphalt mixture under modes I and III. Theoretical and Applied Fracture Mechanics, 2023, 128(4):126-137

[2] Kuchiishi K, Anto C, Vasconcelos K. Influence of viscoelastic properties of cold recycled asphalt mixtures on pavement response by means of temperature instrumentation. Road Materials and Pavement Design, 2019, 20(S2): S710-S724.

[3] Zhu Guodong. Dynamic Viscoelastic Responses of Macro and Meso Structures for Asphalt Concrete. Hefei: Hefei University of Technology,2018.

[4] Benaboud S, Takarli M, Pouteau B. Fatigue process analysis of aged asphalt concrete from two-point bending test using acoustic emission and curve fitting techniques. Construction and Building Materials,2021,301: 124109.

[5] Zhai Wenqing, Li Zhenfeng, Ren Lichao, Xing Jixing, Pang Jinyu. Theoretical and Experimental Data Analysis of Asphalt Viscoelasticity. Journal of Taiyuan University of Science and Technology, 2017, 38(3):233-237.

[6] Yang Shengfeng, Yan Kezhen, Zha Xudong, Li Guokai. Wicket Method of Fractional Derivative Zener Model for Dynamic Viscoelastic of Asphalt Mixture. Highway Engineering, 2022, 47(5):126-131.

[7] Pan Qinxue, Zhenu Jianlong, Yanu Bo, Zha Xudong, Liu Hongfu. Field Prediction Method and Experiment on Creep Response of Asphalt Pavement. China Journal of Highway and Transport, 2017, 30(9):10-17.
[8] You Qinglong, Huang Zhiyi, Wei Binghua, Zhao Shengqian, Yao Yuan. Creep Characteristics of Double Layer Composite Asphalt Mixture. Journal of Materials Science & Engineering, 2023,41(6):1-8.
[9] Mao Bowen. Conversion of Viscoelastic Parameters of Asphalt Mixture and Its Mechanical Influence Analysis. Wuhan, Wuhan Institute of Technology, 2022.
[10] Ma Yunming. Study on indentation creep behavior and viscoelasticity of asphalt mixture. Nanjing, Nanjing Forestry University, 2022.
[11] Underwood B S, Kim Y R, Guddati M N. Improved calculation method of damage parameter in viscoelastic continuum damage model. International Journal of Pavement Engineering, 2010, 11(6): 459-476.
[12] Underwood B S, Baek C, Kim Y R. Simplified viscoelastic continuum damage model as platform for asphalt concrete fatigue analysis. Transportation Research Record,2012,22(96): 36-45.
[13] Roberto A, Romeo E, Montepara A. Effect of fillers and their fractional voids on fundamental fracture properties of asphalt mixtures and mastics. Road Materials and Pavement Design, 2020, 21(1): 25-41.
[14] Hosseini Seyedeh Gashin; Abdi Kordani Ali; Zarei Mohammad. Effect of recycled additives on pure mode I fracture resistance and moisture susceptibility of hot mix asphalt (HMA): An experimental study using semicircular bending (SCB) and indirect tensile strength (ITS) tests. Theoretical and Applied Fracture Mechanics, 2023, 128(4):104-113
[15] Saleh N F, Keshavarzib, Rad F Y. Effects of aging on asphalt mixture and pavement performance. Construction and Building Materials, 2020,258:120309.
[16] Kim M, Phaltane P, Mohammad L. Temperature segregation and its impact on the quality and performance of asphalt pavements. Frontiers of Structural and Civil Engineering, 2018, 12(4):536-547.
[17] Hesami E, Jelagin D, Kringos N. An empirical framework for determining asphalt mastic viscosity as a function of mineral filler concentration. Construction and Building Materials, 2012, 35:23-29.
[18] Ali A, Abbas A, Nazzal M, A.Alhasan. Workability Evaluation of Foamed Warm-Mix Asphalt. Journal of Materials in Civil Engineering, 2013, 26(6):1401-1410.
[19] Liu Jianlan, Wang Chaohui, Wang Xuancang. Mechanical properties of reinforced asphalt concretes with different position grids. Journal of Traffic and Transportation Engineering, 2009, 9(2):22-27.
[20] Zha Xudong, Tanu Tao, Chen Yongqiang, Xie Geng. Experimental analysis of performances for reinforced asphalt pavement with double twisted steel wire mesh. Journal of transport science and engineering,2014,30(1):7-11.